Tunable Magnetism and Half-Metallicity in Hole-Doped Monolayer GaSe

Ting Cao, Zhenglu Li, and Steven G. Louie*
Department of Physics, University of California at Berkeley, Berkeley, California 94720, USA and Material Sciences Division, Lawrence Berkeley National Laboratory, 1 Cyclotron Road, Berkeley, California 94720, USA
(Received 12 September 2014; revised manuscript received 17 March 2015; published 8 June 2015)

We find, through first-principles calculations, that hole doping induces a ferromagnetic phase transition in monolayer GaSe. Upon increasing hole density, the average spin magnetic moment per carrier increases and reaches a plateau near $1.0\,\mu_B$ per carrier in a range of $3 \times 10^{13}/\mathrm{cm}^2 - 1 \times 10^{14}/\mathrm{cm}^2$, with the system in a half-metal state before the moment starts to descend abruptly. The predicted itinerant magnetism originates from an exchange splitting of electronic states at the top of the valence band, where the density of states exhibits a sharp van Hove singularity in this quasi-two-dimensional system.

DOI: 10.1103/PhysRevLett.114.236602 PACS numbers: 72.25.-b, 73.22.-f, 75.70.-i

The study of atomically thin quasi-two-dimensional (2D) crystals has become one of the most rapidly developing areas of condensed matter physics owing to the rich phenomena in and the tremendous promise of applications [1,2] of these materials. The pursuit of controlled magnetism in 2D crystals, in particular, has remained a goal in this area. In graphene, the formation of local magnetic moments and their ordering are theoretically predicted by introducing adatoms, defects, or edges to the system [3–6]. However, experimental measurements of such magnetic moments and the resultant magnetic order often yield ambiguous results [7–12]. Even in its realization, the conducting electrons would only become spin polarized by coupling to localized magnetic moments, and they suffer from significant scatterings by the imperfections introduced. Similar proposals have been put forward for monolayer transition metal dichalcogenides [13], but no experimental evidence of formation of magnetic orders at the single-layer level has been reported so far.

Recently, a new class of 2D crystals, the atomically thin metal monochalcogenides, has attracted much attention [14–22]. In their bulk form, metal monochalcogenides (such as GaS, GaSe, InSe, and GaTe) are layered materials composed of covalently bonded metal and chalcogenide atoms in nanometer-thick layers that are coupled to neighboring layers by weak ionic and van der Waals forces. Like graphene, these materials may be thinned down to form 2D crystals. By using a chemical vapor deposition method, monolayer GaSe has, moreover, been successfully synthesized [17,21,22]. Large-area crystalline GaSe monolayer, which exhibits high photoresponse and p-type transport behavior, can be grown on various substrates [21,22]. The 2D unit cell of a GaSe monolayer is composed of two Ga atoms and two Se atoms. The two neighboring Ga atoms are vertically stacked, and are sandwiched between two planes of Se atoms [Fig. 1(a)]. The in-plane projected geometry of GaSe monolayer crystal forms a honeycomb crystal structure, in which the projected Ga atoms and Se atoms occupy the two triangular sublattices, respectively [Fig. 1(b)].

Although bulk GaSe has a direct band gap according to theoretical calculations [16,21,23], a direct-to-indirect band gap transition occurs as the number of layers is decreased below some critical value, a trend opposite to that of the transition metal dichalcogenides. Specifically, as the number of layers decreases to below 7, calculations show that the conduction band minimum remains at the Brillouin zone center (Γ), but the energy of the states of the highest occupied band near Γ is suppressed, leading to the valence band maximum (VBM) shifting progressively away from Γ to nearby k points, resulting in a Mexican-hat-like energy surface around the zone center [21]. At the monolayer limit, the energy difference between the VBM and the highest valence band state at Γ is maximized, with the Mexican-hat-like landscape extending over a significant fraction of the Brillouin zone. This unusual character of the band structure gives rise in a high density of states (DOS) and an almost one-dimensional-like van Hove singularity near the VBM.

A large DOS at or near the Fermi level (E_F) of a system would, in general, lead to instabilities and transitions to different phases such as magnetism, superconductivity, and other phenomena [3,24,25]. Also, a sharp feature in the DOS near E_F is often indicative of a material with a large

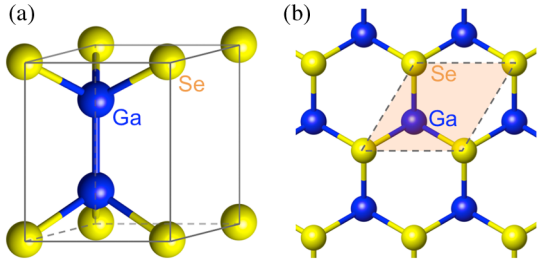

FIG. 1 (color online). The crystal structure of monolayer GaSe. (a) A side view of a unit cell. (b) A top view with the shaded area showing a unit cell.

thermoelectric Seebeck coefficient [26,27]. Here, we report a first-principles theoretical investigation of magnetism in monolayer GaSe as E_F is tuned, via hole doping, through the van Hove singularity in the DOS. We show that there is a Stoner-type magnetic instability with hole doping, leading to a half-metallic ferromagnetic ground state. Ferromagnetism is predicted to appear over a significant range of carrier densities, with the density of magnetic moment and spin-polarized carrier tunable by changing the doping level.

We performed first-principles calculations using density functional theory (DFT) in the local density approximation (LDA) for the exchange-correlation function as implemented in the QUANTUM ESPRESSO package [28]. We employed fully relativistic norm-conserving pseudopotentials, with a plane-wave energy cutoff for the wave functions of 100 Ry. We set the lattice constant to 3.75 Å, corresponding to its experimental measured value for the monolayer and the bulk [21,29]. The atomic positions in the unit cell were fully relaxed until the force on each atom was smaller than 0.01 eV/Å. Since the band structure and the DOS near the VBM are central to the present study, we have also performed quasiparticle band structure calculations within the *ab initio GW* approach [30] as implemented in the BerkeleyGW package [31].

In the calculations, the carrier density was tuned by changing the total number of electrons in the unit cell, with a compensating jellium background of opposite charge added. For various doping conditions, it is found that a minimum number of 8100 (i.e., 90×90) k points was required in sampling the Brillouin zone to converge the magnetic moment, since the magnetic instability depends sensitively on the sampling of the DOS near E_F.

The calculated DFT-LDA Kohn-Sham band structure at zero doping ($p = 0$) is shown in Fig. 2(a), which has an indirect Kohn-Sham band gap of 2.0 eV. At the top valence band, as discussed above, the energy band in the vicinity of the Γ point exhibits a Mexican-hat-like dispersion within a large fraction of the first Brillouin zone. Moving away from the Γ point along different in-plane directions, the energy maxima are almost degenerate. For example, at $p = 0$, the energy maximum along the Γ-K direction is only 0.01 eV higher than that along the Γ-M direction.

A Mexican-hat-like dispersion in two dimensions should give rise to a sharp van Hove singularity in the DOS, resembling that of a band edge in 1D. However, as seen in Fig. 2(b), its divergent behavior in monolayer GaSe is modified by an anisotropic dispersion and spin-orbit splitting which break the cylindrical symmetry of the bands: the DOS is a step function at the VBM and quickly peaks at the energy of 0.013 eV below the VBM. This peak in the DOS originates from saddle critical points of the energy surface for the lower spin-orbit split bands, which are of opposite spin character for the two directions along Γ-K and Γ-K', respectively. A partial density of states

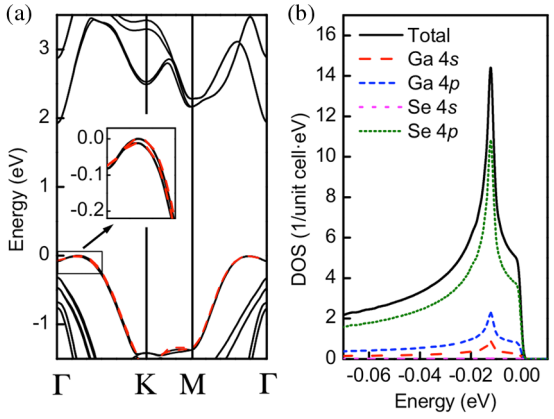

FIG. 2 (color online). Electronic structure of undoped monolayer GaSe. (a) Fully relativistic band structure. The black solid lines are calculated with the LDA functional. The red dashed lines are the top valence bands calculated by the *GW* method. The inset shows the band structure zoomed in near the Γ point. (b) Total and partial density of states near the top of the valence band. As a Gaussian broadening of 0.001 eV is used, the peak in the DOS is finite in the plot.

(PDOS) analysis shows that the DOS near the VBM is mainly composed of Se 4p orbitals, with a small contribution from Ga 4p and 4s orbitals [Fig. 2(b)]. Quite remarkably, from the point of view of the PDOS on each Se atom, it is greater than 2/(eV-atom) for a range of energy near the VBM. This value is comparable to the DOS at E_F of the 3d magnetic transition metals—iron, cobalt, and nickel.

We confirm that the features of the energy dispersion of the top valence bands are robust against many-electron self-energy effects by calculating the quasiparticle band structure. At the G_0W_0 level, we obtain an indirect quasiparticle band gap of 3.7 eV, which is 1.7 eV larger than the LDA Kohn-Sham gap. Despite such a large self-energy correction to the band gap, the dispersion of the *GW* band structure of the top valence bands almost overlaps with the LDA one [Fig. 2(b)]. A detailed analysis around the Γ point shows that the *GW* band structure even has slightly less dispersion [Fig. 2(a), inset], which increases the DOS of the system further as compared to the LDA result.

Although intrinsic monolayer GaSe is nonmagnetic, our relativistic DFT-LDA calculations show that it spontaneously develops a ferromagnetic ground state even at a small amount of hole doping. Figure 3 shows the calculated electron spin magnetic moment per carrier (i.e., $\sum_{n\mathbf{k}\in\text{hole}} - \langle n\mathbf{k}|\mathbf{m}|n\mathbf{k}\rangle / \sum_{n\mathbf{k}\in\text{hole}} \langle n\mathbf{k}|n\mathbf{k}\rangle$, where $\mathbf{m}$ is the spin magnetic moment operator and $|n\mathbf{k}\rangle$ the Bloch states) and the spin-polarization energy per carrier (i.e., the total energy difference between the nonmagnetic and ferromagnetic phase normalized by the number of carriers) as a function of carrier density, for the case with the total electron spin magnetic moment of the system constrained in the out-of-plane direction (along the plane normal). We

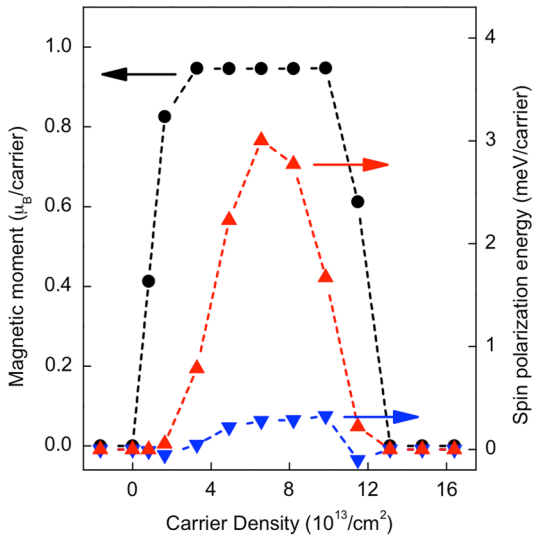

FIG. 3 (color online). Carrier density dependence of spin magnetic moment per carrier and spin-polarization energy per carrier in the out-of-plane spin-polarized ferromagnetic state. Black circles and red triangles denote magnetic moment per carrier and spin-polarization energy per carrier, respectively. Blue inverted triangles denote the magnetic anisotropy energy, defined as the energy difference between the state with out-of-plane polarization and that with in-plane polarization. The data point with negative carrier density corresponds to the electron-doping case.

find an averaged magnetic moment of $0.4\,\mu_B$/carrier at the lowest carrier density considered in our calculations ($p = 8 \times 10^{12}/\mathrm{cm}^2$), with a very small spin-polarization energy (< 0.1 meV/carrier). Larger spin magnetic moment per carrier develops upon increasing carrier density. At $p = 3 \times 10^{13}/\mathrm{cm}^2$, the magnetic moment saturates at nearly $1.0\,\mu_B$/carrier. Provided $p < 1.0 \times 10^{14}/\mathrm{cm}^2$, the magnetic moment per carrier remains at this high value even though the spin carrier density increases by a factor of 3. After this density, further increment of carrier density reduces the magnetic moment per carrier within DFT-LDA. For $p > 1.3 \times 10^{14}/\mathrm{cm}^2$, monolayer GaSe returns to a nonmagnetic state.

In contrast to a nearly constant magnetic moment per carrier above certain carrier density, the spin-polarization energy has a strong dependence on the doping level. Within DFT-LDA, the spin-polarization energy increases monotonically to 3 meV/carrier at $p = 7 \times 10^{13}/\mathrm{cm}^2$, and then, without having a plateau region, decreases monotonically back to 0 at $p = 1.3 \times 10^{14}/\mathrm{cm}^2$.

In our calculations, hole-doped monolayer GaSe exhibits very weak magnetic anisotropy energy. The calculated energy difference between the out-of-plane spin-polarized state and the in-plane spin-polarized state is smaller than 0.3 meV/carrier in all carrier densities considered. The dependence of the anisotropy energy on carrier density is also shown in Fig. 3. At both small and large carrier densities, the out-of-plane spin-polarization orientation is favored over the in-plane spin-polarization orientation, whereas in the intermediate carrier densities, the in-plane spin polarization is favored. The evolution of the magnetic moment per carrier as a function of carrier density for the in-plane spin-polarized ferromagnetic state is very similar to that of the out-of-plane spin-polarized ferromagnetic state shown in Fig. 3.

The physical origin of magnetism upon hole doping for this system can be understood by considering the Stoner mechanism. We calculate the matrix $I_{xc}\chi_0(\mathbf{q})_{\mathbf{G},\mathbf{G}'}$ in the nonmagnetic state, where χ_0 is the noninteracting spin susceptibility in the static limit and I_{xc} the Stoner parameter. An indication for a spontaneous development of magnetization with wave vector $\mathbf{q}$ is that there exists an eigenvalue of the matrix $I_{xc}\chi_0(\mathbf{q})_{G,G'}$ whose module is larger than 1. This condition is equivalent to the traditional scalar Stoner criterion, $I_{xc}\chi_0 > 1$, but generalized to the matrix form which provides a more accurate description of the local fields originating from the nonhomogeneity of the material. At $\mathbf{q} = 0$, the maximum eigenvalue of $I_{xc}\chi_0$ is greater than 1 in doping levels where magnetism emerges, indicative of a tendency toward the formation of a spontaneous ferromagnetic order. Also, the maximum eigenvalues of $I_{xc}\chi_0$ at the center of the Brillouin zone are much larger than those at other regions, suggesting that antiferromagnetism and short-range spin density wave patterns are unfavorable (see Sec. I of Supplemental Material for details [32]).

Ferromagnetism leads to additional exchange splitting of the bands of the two spin types near E_F by the spontaneous breaking of time-reversal symmetry. In Fig. 4, we show the "spin-up" band and the "spin-down" band at $p = 0$ and $7 \times 10^{13}/\mathrm{cm}^2$ for the state constrained with an out-of-plane spin polarization. The spin moment of the Bloch eigenstates is determined by calculating the expectation value of the electron spin magnetic moment operator along the out-of-plane direction using the spinor wave functions. The magnitude of the out-of-plane spin moment of each Bloch eigenstate generally differs from a unit μ_B due to spin-orbit coupling in this material.

A large exchange splitting of the two spin-type bands appears due to a strong exchange field in the ferromagnetic phase [Figs. 4(b) and 4(d)]. At $p = 7 \times 10^{13}/\mathrm{cm}^2$, the additional splitting at the valence band top along the Γ-K direction is 30 meV. This energy corresponds to an effective Zeeman splitting from an external magnetic field of about 260 T, if the orbital magnetic contribution is ignored and a g factor of 2 is assumed. We have also estimated the ferromagnetic transition temperature at $p = 7 \times 10^{13}/\mathrm{cm}^2$. At the mean field level, our estimation yields a transition temperature of about 90 K (see Sec. II of Supplemental Material for details [32]).

As another consequence of the strong exchange splitting of the bands, hole-doped monolayer GaSe in the

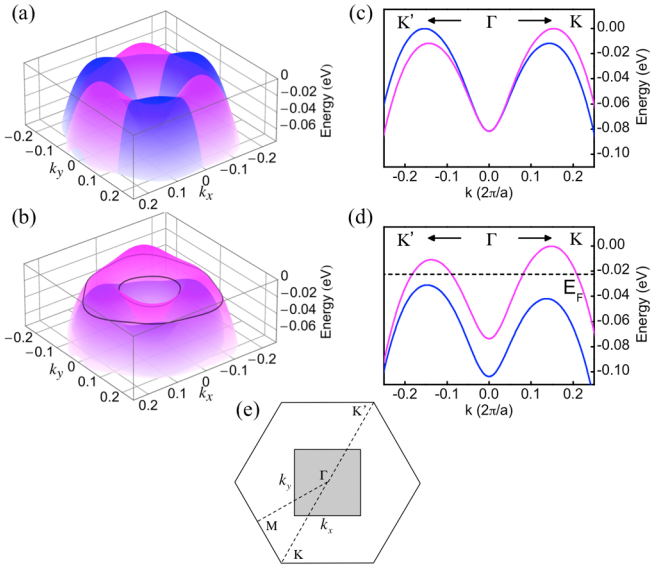

FIG. 4 (color online). Band structure of monolayer GaSe in the out-of-plane spin polarized ferromagnetic state. The purple and blue colors represent spin-up and spin-down electronic states, respectively. (a)–(b) 3D plot of the band structures at carrier density of 0 and $7 \times 10^{13}/\mathrm{cm}^2$, respectively. The black curve denotes the Fermi surface. (c)–(d) Band structures along high-symmetry directions at carrier density of 0 and $7 \times 10^{13}/\mathrm{cm}^2$, respectively. The dashed line denotes the Fermi level. (e) The shaded area shows the k-space area in which (a) and (b) are plotted.

ferromagnetic state is a half metal; i.e., the states at E_F are completely from a band of one spin type (see Sec. III of Supplemental Material for details [32]). In our calculations, at carrier density from $3 \times 10^{13}/\mathrm{cm}^2$ to $1.0 \times 10^{14}/\mathrm{cm}^2$, the Fermi energy only intersects the spin-up band. This half-metallic behavior allows fully polarized spin transport. In addition to the half-metallic behavior, we find a change in the topology of the Fermi surface as the density increases. The shape of the Fermi surface goes from having three pockets at low hole density to a distorted ring at densities between $3 \times 10^{13}/\mathrm{cm}^2$ and $7 \times 10^{13}/\mathrm{cm}^2$.

A key factor to tunable magnetism in monolayer GaSe is the controllability of carrier density at relatively high doping levels. For this purpose, atomically thin materials offer a great advantage compared to bulk materials. Because of their thinness, doping carrier densities have been achieved to the order of $10^{14}/\mathrm{cm}^2$ in graphene by ion liquid gating [33,34] and to $10^{13}/\mathrm{cm}^2$ in transition metal dichalcogenide monolayers by back-gate gating [35,36]. We therefore expect that tunable hole doping, to the level discussed in this Letter, can also be readily achieved for monolayer GaSe with currently available gating techniques. The introduction of p-type dopants and defects may also be a viable means towards achieving the predicted magnetic state. From calculations on substitutional doping with a portion of Se atoms replaced by As atoms in a large supercell, we find that ferromagnetism and similar magnetic properties arise at doping levels discussed in the above calculations with electrostatic doping (see Sec. IV of Supplemental Material for details [32]).

The predicted spontaneous magnetization upon hole doping should be detectable in monolayer GaSe by various methods. In transport measurements, the resistance in the ferromagnetic state is spin dependent for single-domain samples. Direct detections of the spin polarization employing spin-polarized scan probes such as spin-polarized scanning tunneling microscope or optical measurements such as the magneto-optic Kerr effect can also give evidence of magnetization. In addition, as seen in Fig. 1(b), monolayer GaSe does not have inversion symmetry. The Berry curvature is thus generally nonvanishing in the 2D Brillouin zone in the undoped case [37,38]. This property, together with the doping-dependent Fermi surface topology and band splitting, may give rise to anomalous Hall and spin-Hall currents in this interesting 2D system.

Moreover, as bulk GaSe is a weakly coupled layered material, the interlayer electronic coupling strength is weak. Consequently, multilayer GaSe with different interlayer stacking configurations or intercalated bulk GaSe samples may offer tunable magnetic properties similar to its monolayer form. We would also like to point out that GaSe is but one of the many layered metal monochalcogenides. Materials such as monolayer GaS and GaTe all have similar crystal and electronic structures [19]. The variety of materials in this family offers a great opportunity to explore magnetic phenomena in 2D.

In conclusion, we find through first-principles calculations that hole doping induces tunable ferromagnetism and half-metallicity in monolayer GaSe. For a range of hole carrier density, the averaged electron spin magnetic moment can be as large as nearly $1.0\,\mu_B$/carrier. We demonstrate that this itinerant magnetism originates from a Stoner mechanism with an exchange-field splitting of the electronic states near the VBM, where the DOS for this 2D material is very high and exhibits a sharp van Hove singularity. Our findings not only reveal, for the first time, the possibility of doping-induced tunable magnetism in quasi-2D semiconductors, but also may open up an opportunity to realize spintronics at the atomically thin single-layer level, in which controlled spin moment and transport may be achieved by electrostatic gating.

We thank J. Lischner and Y. M. Lu for helpful discussions. This research was supported by the Theory Program at the Lawrence Berkeley National Lab through the Office of Basic Energy Sciences, U.S. Department of Energy under Contract No. DE-AC02-05CH11231, which provided the GW calculations, and by the National Science Foundation under Grant No. DMR10-1006184, which provided for the DFT study of doping-induced magnetism. This research used resources of the National Energy

Research Scientific Computing Center, which is supported by the Office of Science of the U.S. Department of Energy.

Note added.—After submission of this letter, an article has appeared on a complimentary study discussing *p*-type vacancy-induced magnetism in monolayer GaSe and GaS [39].

*sglouie@berkeley.edu

[1] Q. H. Wang, K. Kalantar-Zadeh, A. Kis, J. N. Coleman, and M. S. Strano, Nat. Nanotechnol. **7**, 699 (2012).
[2] A. K. Geim and I. V. Grigorieva, Nature (London) **499**, 419 (2013).
[3] Y. W. Son, M. L. Cohen, and S. G. Louie, Nature (London) **444**, 347 (2006).
[4] O. Yazyev and L. Helm, Phys. Rev. B **75**, 125408 (2007).
[5] D. Boukhvalov, M. Katsnelson, and A. Lichtenstein, Phys. Rev. B **77**, 035427 (2008).
[6] O. Yazyev, Phys. Rev. Lett. **101**, 037203 (2008).
[7] J.-H. Chen, L. Li, W. G. Cullen, E. D. Williams, and M. S. Fuhrer, Nat. Phys. **7**, 535 (2011).
[8] B. Dlubak *et al.*, Nat. Phys. **8**, 557 (2012).
[9] K. M. McCreary, A. G. Swartz, W. Han, J. Fabian, and R. K. Kawakami, Phys. Rev. Lett. **109**, 186604 (2012).
[10] R. R. Nair, M. Sepioni, I. L. Tsai, O. Lehtinen, J. Keinonen, A. V. Krasheninnikov, T. Thomson, A. K. Geim, and I. V. Grigorieva, Nat. Phys. **8**, 199 (2012).
[11] M. Lundeberg, R. Yang, J. Renard, and J. Folk, Phys. Rev. Lett. **110**, 156601 (2013).
[12] T. Maassen, J. van den Berg, E. Huisman, H. Dijkstra, F. Fromm, T. Seyller, and B. van Wees, Phys. Rev. Lett. **110**, 067209 (2013).
[13] Y. Cheng, Z. Zhu, W. Mi, Z. Guo, and U. Schwingenschlögl, Phys. Rev. B **87**, 100401 (2013).
[14] P. Hu, Z. Wen, L. Wang, P. Tan, and K. Xiao, ACS Nano **6**, 5988 (2012).
[15] D. J. Late, B. Liu, J. Luo, A. Yan, H. S. Matte, M. Grayson, C. N. Rao, and V. P. Dravid, Adv. Mater. **24**, 3549 (2012).
[16] Z. Zhu, Y. Cheng, and U. Schwingenschlögl, Phys. Rev. Lett. **108**, 266805 (2012).
[17] S. Lei, L. Ge, Z. Liu, S. Najmaei, G. Shi, G. You, J. Lou, R. Vajtai, and P. M. Ajayan, Nano Lett. **13**, 2777 (2013).
[18] H. L. Zhuang and R. G. Hennig, Chem. Mater. **25**, 3232 (2013).
[19] V. Zólyomi, N. D. Drummond, and V. I. Fal'ko, Phys. Rev. B **87**, 195403 (2013).
[20] P. Hu *et al.*, Nano Res. **7**, 694 (2014).
[21] X. Li *et al.*, Sci. Rep. **4**, 5497 (2014).
[22] Y. Zhou, Y. Nie, Y. Liu, K. Yan, J. Hong, C. Jin, Y. Zhou, J. Yin, Z. Liu, and H. Peng, ACS Nano **8**, 1485 (2014).
[23] Y. Ma, Y. Dai, M. Guo, L. Yu, and B. Huang, Phys. Chem. Chem. Phys. **15**, 7098 (2013).
[24] E. V. Castro, N. M. R. Peres, T. Stauber, and N. A. P. Silva, Phys. Rev. Lett. **100**, 186803 (2008).
[25] J. Bardeen, L. N. Cooper, and J. R. Schrieffer, Phys. Rev. **108**, 1175 (1957).
[26] J. P. Heremans, V. Jovovic, E. S. Toberer, A. Saramat, K. Kurosaki, A. Charoenphakdee, S. Yamanaka, and G. J. Snyder, Science **321**, 554 (2008).
[27] M. S. Dresselhaus, G. Chen, M. Y. Tang, R. G. Yang, H. Lee, D. Z. Wang, Z. F. Ren, J. P. Fleurial, and P. Gogna, Adv. Mater. **19**, 1043 (2007).
[28] P. Giannozzi *et al.*, J. Phys. Condens. Matter **21**, 395502 (2009).
[29] A. Kuhn, A. Chevy, and R. Chevalier, Phys. Status Solidi A **31**, 469 (1975).
[30] M. Hybertsen and S. G. Louie, Phys. Rev. B **34**, 5390 (1986).
[31] J. Deslippe, G. Samsonidze, D. A. Strubbe, M. Jain, M. L. Cohen, and S. G. Louie, Comput. Phys. Commun. **183**, 1269 (2012).
[32] See Supplemental Material at http://link.aps.org/supplemental/10.1103/PhysRevLett.114.236602 for Stoner mechanism of magnetic instabilities, estimation of ferromagnetic transition temperature, carrier density dependent band structure, and magnetism from substitutional dopants.
[33] D. K. Efetov and P. Kim, Phys. Rev. Lett. **105**, 256805 (2010).
[34] J. Ye, M. F. Craciun, M. Koshino, S. Russo, S. Inoue, H. Yuan, H. Shimotani, A. F. Morpurgo, and Y. Iwasa, Proc. Natl. Acad. Sci. USA **108**, 13002 (2011).
[35] K. F. Mak, K. He, C. Lee, G. H. Lee, J. Hone, T. F. Heinz, and J. Shan, Nat. Mater. **12**, 207 (2013).
[36] Y. J. Zhang, T. Oka, R. Suzuki, J. T. Ye, and Y. Iwasa, Science **344**, 725 (2014).
[37] T. Cao *et al.*, Nat. Commun. **3**, 887 (2012).
[38] D. Xiao, G.-B. Liu, W. Feng, X. Xu, and W. Yao, Phys. Rev. Lett. **108**, 196802 (2012).
[39] S. Wu, X. Dai, H. Yu, H. Fan, J. Hu, and W. Yao, arXiv:1409.4733.